Hindawi
Mathematical Problems in Engineering
Volume 2022, Article ID 9928041, 13 pages
https://doi.org/10.1155/2022/9928041

Research Article

3D Image Based on Visual Sensor in Public Space Landscape Model

Tengjiao Liu

College of Arts, Xi'an Fanyi University, Xi'an 710105, Shaanxi, China

Correspondence should be addressed to Tengjiao Liu; liutengjiao@xafy.edu.cn

Received 17 March 2022; Revised 7 May 2022; Accepted 20 May 2022; Published 30 July 2022

Academic Editor: Zhihan Lv

With the rapid development of the times, the computing of the internet of things and the industry go hand in hand, the application of visual sensors is becoming more and more extensive, and the image fusion technology and target recognition technology have been further improved. It can be said that it is a hot topic at home and abroad high-end technology. With the continuous improvement of people's living standards, the specific requirements for the quality of life are gradually increasing. The landscape construction of public space has become a topic of discussion. People are becoming more and more stringent about the landscape environment around them. Landscape designers also feel distressed by this and pursue this higher level, which can not only improve the living environment, but also make people being able to live and work in peace, and contentment is an honor for the landscape architect. Therefore, this study builds an excellent public space landscape model based on the 3D image processing of the visual sensor, establishes the coverage relationship table through the genetic algorithm and the greedy algorithm, and then uses the infrared image segmentation method of the local entropy combined with the region growth method to segment the 3D image of the vision sensor. Then, we use the multi-image fusion method based on the dimensional closeness to merge and finally analyze the public space landscape model with extremely high integrity. Moreover, this study also discusses the analysis results of temperature and time on the integrity of the landscape model. Between 35.5°C and 36.7°C, from 12 o'clock to 14 o'clock, the integrity of the public space landscape model is as high as 97.2%.

1. Introduction

Over the years, with the development of the computing and industry of the internet of things, visual sensor networks have been widely used. The image fusion technology and target recognition technology of the visual sensor network are common and important technologies that much related personnel pay attention to in the world. Overseas, they continue to invest in a lot of materials and financial resources, and they will receive more attention in future applications. With the rapid development of our country's economic structure, people's living standards have continued to improve, and people's attention to the surrounding environment has also increased. Living space with fresh air and an elegant environment is urgently needed by people. How to create an environment that can not only meet functional requirements but also make people feel more comfortable in the outdoor public space? This is a topic of very intensive investigation and research in landscape art.

Therefore, starting from the visual sensor, this study analyzes the 3D image and establishes the public space landscape model. The visual node perception model of visual sensor networks is a directional perception model, and the vision of nodes is limited, so the extended nodes cannot be static. Generally speaking, nodes are divided into the following three categories: rotatable, movable, and rotatable. This vision sensor network is called a dynamic vision sensor network (dynamic vision sensor network, DVSN). At the same time, it has the characteristics of a visual sensor network and mobile sensor network, and its research and application value is also very high. If the algorithm covers multiple nodes with the most target points, we use the random method to select nodes. This will affect the coverage effect. Therefore, the "contribution rate" model is imported, and coverage works first. We optimize network coverage and solve node coverage conflicts at the same time. This study will study the processing of 3D images using vertical and horizontal vision sensors. First, we start from the vertical

sequence of the historical development and evolution of public space, and sort out the evolution and reasons for the landscape design of public space. The current situation of public space design is the starting point. From the perspective of landscape architecture, this study comprehensively analyzes the problems and solutions of current public space design, such as website selection, scale, layout, and vegetation design. This study advocates the beautiful vision of public space and designs the landscape orientation of public space in the future. First, we should change our consciousness, protect the tradition, develop innovation at the same time, and finally establish the public space in the village, the most suitable place for residents.

In daily life, there are many kinds of pipeline defects, the detection is difficult, and the degree of automation is low. In this work, Yang et al. [1] proposed a new omnidirectional visual inspection system for detecting morphological defects. He designed an active stereo omnidirectional vision sensor to obtain real-time texture and depth information of the inner wall of the pipeline [1]. He makes good use of the application of vision sensors in 3D images, but it is limited to pipeline surveys. In recent years, the use of computer vision technology to study the deformation of objects has been in-depth research. A widely used technique is 3D nonrigid registration, which is used to estimate the transformation between two instances of deformed structures. Although there are many previous developments on this subject, it is still a challenging problem. Saval-CalvoM proposes a new method that combines nonrigid registration of two data spaces in order to robustly calculate the correspondence and conversion between the two datasets [2]. The new method of combining two data spaces proposed by Saval-CalvoM is very novel, which is of great help to image recognition, but the application of visual sensors is not adequate. Pujol-MiroA proposed a new method based on a convolutional neural network (CNN), which can obtain the corresponding matching between the key point sets captured by multiple unorganized 3D point clouds independent of the sensors used [3]. The CNN method He proposed is very good at capturing 3D features, but the acceptance of it is a bit lagging behind. Vision sensors still have many uses. For example, they have great potential in surveying. Li and Zhong's [4] research aims to find feasible accurate navigation models for the planned lunar rover. Autonomous navigation is one of the most important tasks in China's lunar exploration project [4]. The whole process is very smooth, and the use of vision sensors is quite skillful. With the development of computer vision technology, 3D reconstruction has become a hot spot. At present, 3D reconstruction heavily relies on expensive equipment, and the real-time performance is poor. Li et al [5] aim to solve the 3D reconstruction problem of indoor scenes with large vertical span and propose a new method of 3D reconstruction of indoor scenes using Kinect only [5]. It perfectly solves the 3D reconstruction problem, but there is almost no use of visual sensors. The LIRIS demonstrator is a vision-based navigation sensor experiment, implemented on ATV-5 George Lemaitre and activated during the approach phase with the International Space Station (ISS). Research on noncooperative junction points emphasizes the need for GNC based on image processing using LiDAR sensors and cameras. During the ATV-5 approach, Masson A used two infrared cameras, a monochromatic visible-light camera, and a scanning LiDAR to fly off the special International Space Station and recorded images during the meeting with the International Space Station that ended in docking [6]. This is the use of vision sensors in aviation. Validating the long-term biomass prediction of the forest landscape model (FLM) has always been a challenging task. Ma J uses a spatiotemporal alternative method to generate a curve of forest biomass with forest age from the forest survey data set (FSD) of the Xiaoxing'an Mountains (LKM) in Northeast China and compares the model with the long-term biomass prediction of LANDIS-II (7). He refers to the forest landscape model, but it has nothing to do with visual sensing. With the rapid development of urbanization and industrialization, China is paying more and more attention to air quality. As an important air pollutant, PM2.5 has received extensive attention. Urban green space, which is a seminatural surface landscape, will affect the concentration and distribution of PM2.5. The current research mainly focuses on the microscale, and there is almost no research on the scale of the landscape. Li Q uses a land-use regression (LUR) model to increase the density of monitoring points. According to the usual timing interpolation method, the spatial distribution of PM2.5 concentration is simulated with high precision [7, 8]. Based on the landscape model to analyze the relationship between PM2.5 concentration and green space, Li et al.'s [8] idea is very clever, but the 3D image recognition technology is not mentioned, and the reference is not great.

The innovation of this study is to explain the process of this infrared image segmentation method in detail.

The advantages of this method are shown by comparing the commonly used image detection and image segmentation methods and experiments. The SIFT algorithm is used to extract the feature points of the image. After describing the feature points, the conversion relationship between images is found according to the feature points. The conversion calculated value is used to perform coordinate transformation and map the points on the image. Then, in order to realize image position alignment, a multisensor consistency reliability fusion method based on interpolation and extended dimension proximity is proposed. Then, this method is suitable for image fusion at the pixel level, and then, a multi-image fusion method based on extended dimension proximity is proposed. Finally, several registered images are used for fusion experiments to compare the effect of the average image fusion method. The advantages of this method are proved by vision, evaluation benchmark of sensory and fused images. Second, according to the progress of relevant research at home and abroad, this study analyzes the current situation of the formation space of eye illusion and the reference methods at home and abroad, defines the significance, expansion, and principle of eye illusion, defines the factors and types of eye illusion, and studies the theoretical basis of the eye-illusion design of environmental action psychology, including landscape ecology and other public space landscapes. We explore the method of eye-illusion design of public space landscape and use space, color, material, light and shadow, disintegration, and three-dimensional painting to design the landscape of fantasy space.

2. Method for Establishing a Public Spatial Landscape Model Based on Visual Sensor 3D Images

2.1. Visual Sensor Network

2.1.1. Basic Structure of Visual Sensor Network. The vision sensor is the direct source of information for the whole machine vision system [9]. It is mainly composed of one or two graphic sensors, and is sometimes equipped with light projectors and other auxiliary equipment. The visual sensor network is a new type of network [10], which adds audio, video, image, and other multimedia information collection on the basis of the traditional sensor network, so as to better complete the monitoring task. The vision sensor nodes (Vision Sensor Nodes) in the network are equipped with miniature CMOS cameras, miniature microphones, and other sensors with environmental information perception functions [11]. They are generally arranged in unattended areas to complete monitoring or monitoring tasks. The basic structure of the visual sensor network [12] is shown in Figure 1:

2.1.2. Vision Sensor Node Structure. Like traditional sensor nodes, vision sensor nodes also follow the design principles of low power consumption, low cost, and miniaturization. The general nodes are composed of data acquisition units, data processing units, data transmission, and energy management modules, as shown in Figure 2.

The data acquisition unit includes a micro-CMOS camera [13] and other commonly used scalar information (such as temperature and humidity) sensors, which are mainly responsible for the collection and data conversion of environmental information in the monitoring area; the data processing unit is mainly responsible for the data collected that perform processing (such as compression coding), store the data in the sending buffer, call the data transmission module to transmit data, and also undertake the task of controlling node operations; the data transmission unit is mainly responsible for wireless communication with other nodes to achieve data exchange.

2.1.3. Characteristics of Visual Sensor Network. The visual sensor network is a new type of surveillance network [14]. In addition to the same characteristics as the traditional sensor network, it also has its own unique characteristics as follows:

(1) Rich media is perceived. There are multiple data types such as video, audio, image, and numerical value in the visual sensor network, which include not only streaming media information but also some scalar data information [15].

(2) Network capabilities are enhanced. A large amount of streaming media information has been introduced into the visual sensor network. Due to the large amount of data contained in this information, visual sensor nodes have significantly enhanced network capabilities such as information collection, data processing and storage and forwarding, and node energy supply [16].

(3) Complex processing tasks. In traditional wireless sensor networks, the collected information is often only simple environmental information, the data structure is simple, the amount of data is also small, the processor is not demanding, and often only some simple calculations are needed to complete the processing tasks [9].

A 3D image processing method, which is characterized in that at least one image container, is created. The image container has a display dimension identification and a coverage area identification. The displayed image is displayed in the image container corresponding to the display dimension ID and coverage area ID.

2.2. Theoretical System of Landscape Architecture

2.2.1. Concept of Landscape Architecture. Landscape design is the science and art of landscape analysis, planning, layout, design, conversion, management, protection, and restoration. Some experts believe that the meaning of landscape is very broad. It is a trace of complex natural processes and human activities on the Earth, and it is a carrier of multiple functions (processes). In short, excellent landscape design is not only economically beautiful but also protects the ecological environment [17]. However, ecology and landscape design are different. Landscape design emphasizes the planning and design of the land, and proposes a solution to the problem of the site, but landscape ecology emphasizes the spatial pattern and ecological process of the ecosystem in a wider space and time.

2.2.2. Elements of Landscape Architecture. John Simmons divided the main elements of landscape design into climate, soil, water, plants, topography, transportation, structure, and other elements. Among them, climate and soil are constant factors of the landscape, which cannot be changed by human beings.

(1) Terrain. Topographic elements are the first elements considered in landscape design. To draw a topographic map, the terrain, vegetation, water system, surrounding structures, and traffic routes must be clearly stated. There are countless examples of using topography for excellent design. The most famous is the clever design of cliffs and water currents flowing at the bottom of buildings.

(2) Water. "Water" is the most spiritual element of the landscape, and it can make a space become active, can attract people's participation, and make the space full of charm. The use of water elements can make hydrophilic, static waterscape, dynamic waterscape, and ecological landscape design types.

(3) Vegetation. Yu Kongjian once said that when we do not know how to continue in the design process, we will ask for multiple trees. "Planting trees" shows the importance of plants in landscape design. Plants are the most colorful elements in the space composition. There are many types and different times. In short, the selection of each plant must

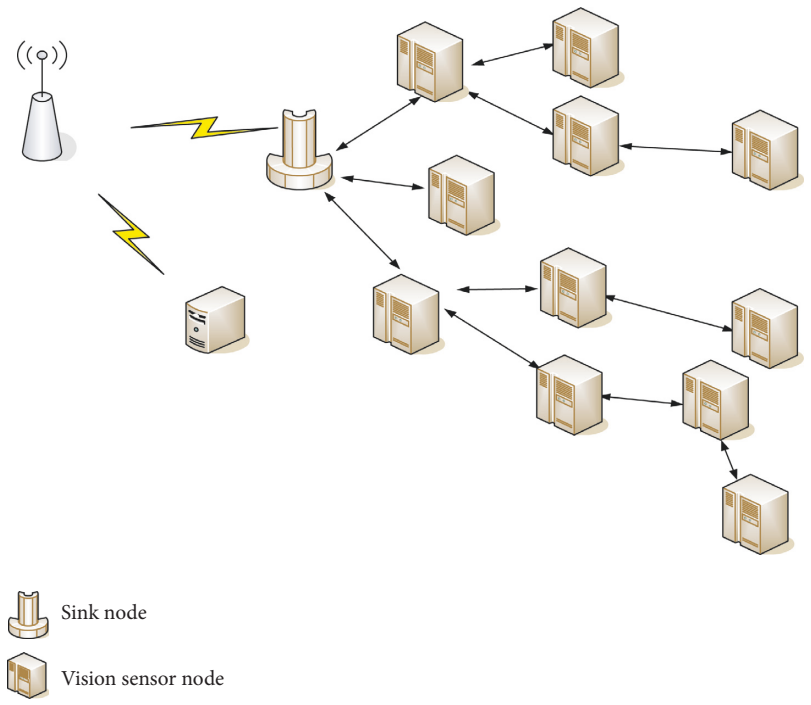

Figure 1: Basic structure of visual sensor network.

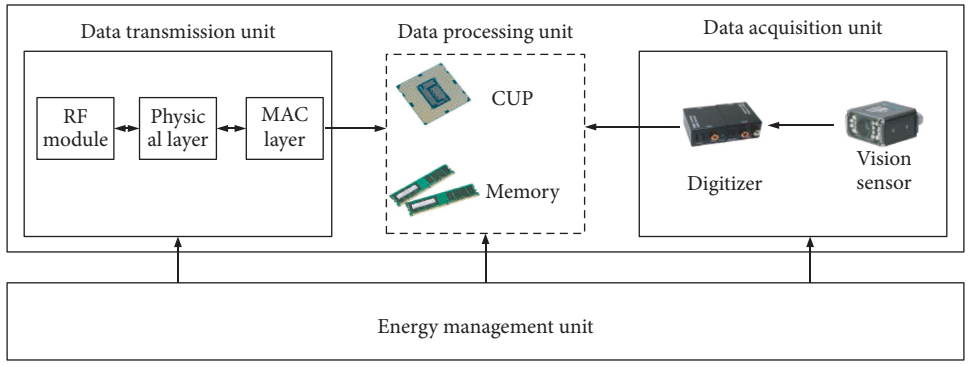

Figure 2: Vision sensor node structure.

consider its characteristics, such as shape, height, crown width, color, flowering season, and evergreen leaves, and design and match by comprehensively weighing the characteristics of each plant species.

(4) Transportation. Roads are one of the important elements in landscape design. Roads are divided into main roads, secondary roads, garden roads, etc. The design should first clarify the site traffic relationship. The road is the structural framework of a plot. What kind of road is designed the direction means to create what kind of plane layout.

In summary, all the constituent elements of landscape design are to create a more healthy and vibrant environment and create a harmonious lifestyle.

2.3. Plane Optical Illusion. The causes of visual illusions are quite complex. It exists not only in our gestures but also in the external projection of people's abstract heart. When people see flat geometric figures, due to psychological factors, there is an illusion of relationship between lines and figures. Geometric features are specific directions, lengths, angles, areas, and curvatures, and these geometric features will produce changes that contradict changes in objective facts, which are collectively referred to as plane illusions [18]. Plane visual illusions generally include the following categories:

2.3.1. Optical Illusion of Direction. In the plane graphics, the visual perception of the lines and the direction of the graphics do not match the objective facts. As shown in Figures 3(a)–3(c), there are three types of directional optical illusion [19].

2.3.2. Long and Short Optical Illusion. As shown in Figure 4, Fick's optical illusion [20], the two line segments in the figure have the same length, but the viewer will feel that the vertical

line is longer than the horizontal line due to the influence of the placement method. Also shown in Figure 4, there is the optical illusion of Muller-Lyer. The two line segments in the picture are of equal length. The upper line segment has arrow tails at both ends, and the lower line segment has arrow signs.

2.3.3. Optical Illusion of Bending. This type of optical illusion refers to the phenomenon that the plane graphics are visually distorted due to the influence or interference with the surrounding graphics. As shown in Figure 5, the Black Forest optical illusion, the parallel lines in the figure are interfered with by two sets of rays, which make the viewer feel that the middle section of the parallel design lines has curved outward, respectively. Contrary to the Black Forest illusion, in the Wundt optical illusion as shown in Figure 5, the parallel lines produce an inwardly curved arc.

The application of visual illusion in visual communication design can not only promote the progress of society but also improve the quality of public life, so as to serve the public. The application of visual illusion in visual communication reflects its high value.

2.4. Infrared Image Segmentation and Target Object Extraction

2.4.1. Infrared Image Segmentation Method. With the rapid development of infrared technology, infrared imaging systems are widely used in the military and civilian fields. The strong anti-interference ability and the advantages of being unaffected by light when working make it play a key role in many fields. The 3D packaging refers to the 3D integration (3D Integration) scheme, which relies on traditional interconnection methods (such as wire bonding and flip chip) to realize vertical stacking at the packaging level. Examples of 3D packaging include a stacked package (POP) that encapsulates a single chip and then stacks the packages and interconnects them through a wire bonding or flip-chip process, and forming an interconnected 3D wafer-level package (3D WLP) using a redistribution layer (RDL) and a bump process.

The idea of the new method of infrared image segmentation [21, 22] is as follows: first, the image is subjected to Butterworth high-pass filtering, and the infrared high-brightness part is extracted and superimposed on the original image to achieve the purpose of the image enhancement; then, the image local entropy is calculated and generated local entropy image, because the outer contour of the local entropy image is usually larger than the actual contour, so one more erosion operation is used to eliminate the excessive outer contour, and the optimized template is obtained; finally, the template is superimposed with the original image, and the black area is negated to obtain the target image. The method flow is shown in Figure 6.

2.4.2. The Basic Law of Infrared Radiation. When the temperature of an object is higher than the absolute temperature, its internal molecules and atoms will randomly move, and the surface will radiate infrared rays. The following are the three basic laws of infrared radiation [23–25].

(1) Planck's Law of Radiation. The power W_λ per unit surface area radiated to the entire hemispherical space at unit wavelength is

$$W_\lambda = \frac{2\pi hc^2}{\lambda^5}\left[\exp\left(\frac{hc}{\lambda kT}\right) - 1\right]^{-1}. \quad (1)$$

In the formula, c is the speed of light in vacuum $(2.997 * 10^8\ \mathrm{ms}^{-1})$, h is Planck's constant $(6.626 * 10^{-34}\ \mathrm{js})$, k is Boltzmann's constant $(1.381 * 10^{-23}\ \mathrm{JK}^{-1})$, T is the absolute temperature (K), and λ is the radiation wavelength (m).

(2) Stefan-Boltzmann's Law. The total power W radiated by the blackbody in the upper hemisphere space per unit area is as follows:

$$W = \int_0^\infty W_\lambda \mathrm{d}\lambda = \sigma T^4. \quad (2)$$

where σ is the Stefan-Boltzmann constant $(5.6697 * 10^{-8}\ \mathrm{w}/(\mathrm{m}^2\mathrm{K}^4))$.

(3) Lambert's Cosine Law. The radiation intensity of a blackbody in any direction is proportional to the cosine value of the angle α between the observation direction and the normal of the radiation surface, as shown in Figure 7.

$$I_\alpha = I_0 \cos\ \alpha. \quad (3)$$

This law shows that the blackbody has the strongest radiation in the normal direction of the radiation surface.

The radiation intensity is also related to the emissivity. The radiation intensity is the object's radiative blackbody radiation term multiplied by the object's spectral emissivity $\varepsilon(\lambda)$.

$$[W(\lambda, T)] = \varepsilon(\lambda, T) W(\lambda, T). \quad (4)$$

The heat radiation generated by the friction between the aircraft and the atmosphere and the heat radiation emitted by the aircraft engine are higher than the surrounding background, which is reflected in the infrared image. The stronger the heat radiation, the higher the pixel gray value, so that the target can be well located. We extract the pixel coordinates with the highest gray value by traversing the picture, as the seed point coordinates of the region growth.

Infrared radiation can be divided into several different bands according to the wavelength. During imaging, due to the characteristics of infrared radiation and imaging detector, infrared images can only output images of a specific band at a time. Therefore, images of other bands can be obtained from one band through band expansion, which is of research value for the research and development, performance evaluation, and improvement of various infrared equipment.

2.4.3. Mathematical Model of Line-Structured Light Sensor. In the sensor measurement [26], there are two coordinate systems, the coordinate system $O_a - X_a Y_a Z_a$ of the light projection plane and the coordinate system $O_c - X_c Y_c Z_c$ of the camera, as shown in Figure 8, which will be replaced by coordinate system T_1 and coordinate system T_2 in the following text.

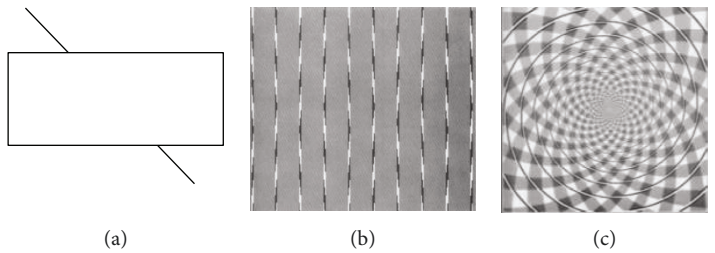

Figure 3: Three types of directional optical illusions. (a) Poggendorff optical illusion. (b) Zollner optical illusion. (c) Fraser optical illusion.

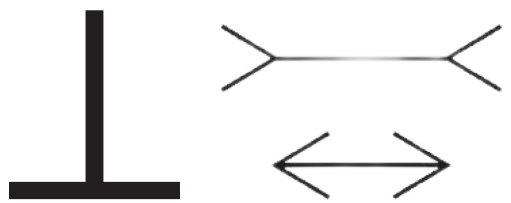

Figure 4: Two long and short optical illusions. (a) Fick's optical illusion. (b) Müller-Lyer's optical illusion.

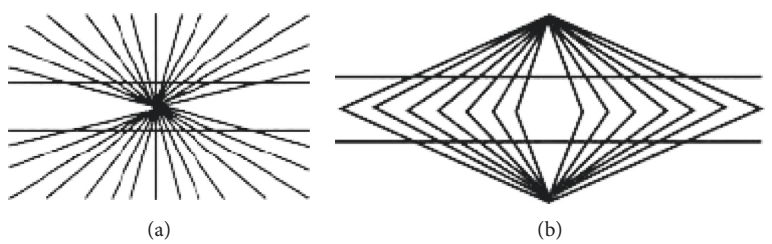

Figure 5: Two kinds of curved optical illusions. (a) Black Forest optical illusion. (b) Wundt optical illusion.

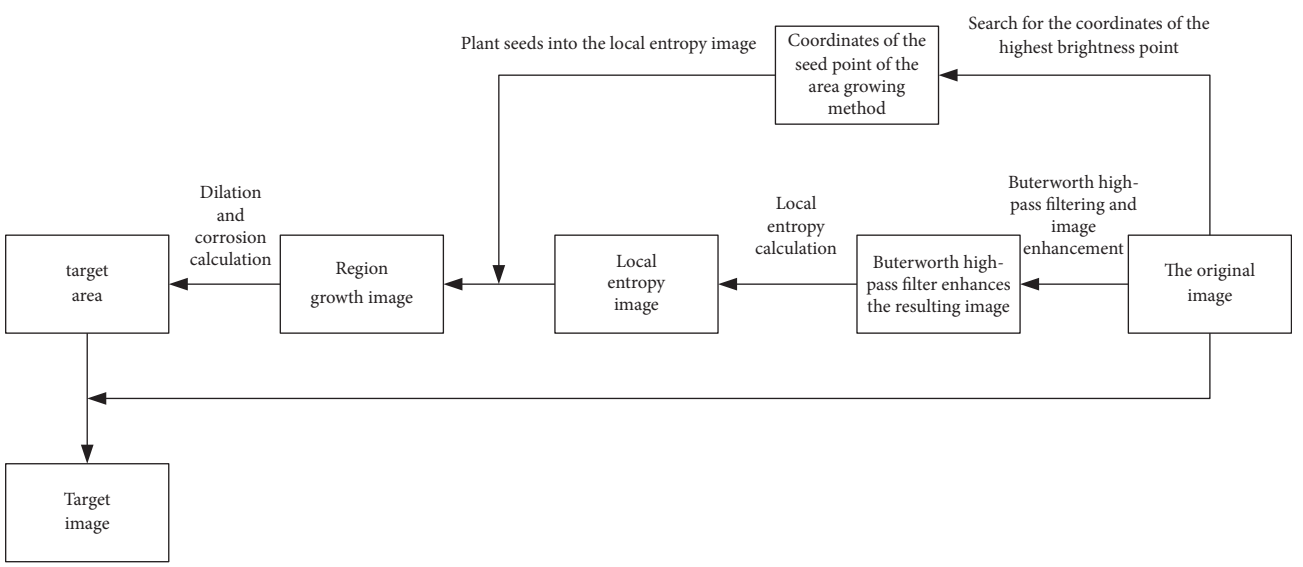

Figure 6: Flowchart of target image extraction.

The coordinates of the measurement data obtained by the sensor are based on the coordinate system T_1, and the equation of the projection curve can be expressed as follows:

$$\begin{aligned} X_a &= 0, \\ Z_a &= f\left(X_a, Y_a\right). \end{aligned} \tag{5}$$

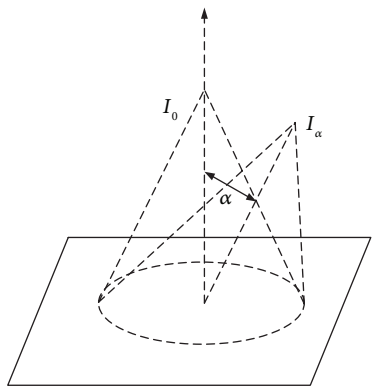

Figure 7: The spatial distribution of radiation.

To transform the coordinates in the image coordinate system to the coordinate system T_1, the following transformations are required: we first transform the coordinate system T_1 to the coordinate system T_2 O_a, that is, translate the coordinate system origin T_2 to the coordinate system O_a origin, then rotate around the X_a axis 180°, and then rotate around the Y_a axis -α angle; then the coordinate system T_2 is transformed into the image coordinate system through perspective projection transformation. Then, the conversion relationship between the coordinate system T_1 and T_2 is as follows:

$$V_j = HV_aH = P * R_{x_a}(\alpha) * R_{y_a}(180^\circ), \tag{6}$$

where P is the perspective transformation matrix, which is expressed as follows:

$$P = \begin{bmatrix} f & 0 & 0 & 0 \\ 0 & f & 0 & 0 \\ 0 & 0 & f & 0 \\ 0 & 0 & 1 & f \end{bmatrix}, \tag{7}$$

T_i is the translation matrix, which is expressed as follows:

$$T_i = \begin{bmatrix} 1 & 0 & 0 & -D_{pc} \\ 0 & 1 & 0 & 0 \\ 0 & 0 & 1 & -D_{pg} \\ 0 & 0 & 0 & 1 \end{bmatrix}. \tag{8}$$

The two rotation matrices $R_{Y_a}(-\alpha)$ and $R_{X_a}(180^\circ)$ are as follows:

$$R_{Y_a}(-\alpha) = \begin{bmatrix} \cos\alpha & 0 & \sin\alpha & 0 \\ 0 & 1 & 0 & 0 \\ -\sin\alpha & 0 & \cos\alpha & 0 \\ 0 & 0 & 0 & 1 \end{bmatrix} R_{X_a}(180^\circ) = \begin{bmatrix} 1 & 0 & 0 & 0 \\ 0 & -1 & 0 & 0 \\ 0 & 0 & -1 & 0 \\ 0 & 0 & 0 & 1 \end{bmatrix}. \tag{9}$$

Solving equation (6), we can get the following:

$$V_a = H^{-1} * V_i = T_i^{-1} * R_{X_a}(180^\circ)^{-1} * R_{Y_a}(-\alpha)^{-1} * p^{-1}. \tag{10}$$

$$H^{-1} = \frac{1}{f^2} \begin{bmatrix} f \cdot \cos\alpha & 0 & -f \cdot \sin\alpha - D_{pc} & f \cdot D_{pc} \\ 0 & -f & 0 & 0 \\ -f \cdot \sin\alpha & 0 & -f \cdot \cos\alpha - D_{pa} & f \cdot D_{pa} \\ 0 & 0 & -1 & f \end{bmatrix}. \tag{11}$$

From equation (5), we can get the following:

$$\begin{bmatrix} X_a \\ Y_a \\ Z_a \\ 1 \end{bmatrix} = H^{-1} \begin{bmatrix} X_i \\ Y_i \\ Z_i \\ 1 \end{bmatrix}. \tag{12}$$

We take equation (11) into equation (12) to get the following:

$$\begin{cases} X_a = \dfrac{X_i f \cos\alpha - \left(f \sin\alpha + D_{pc}\right) Z_i + f D_{pc}}{f - Z_i} \\ Y_a = \dfrac{-f}{f - Z_i} Y_i \\ Z_a = \dfrac{-X_i f \sin\alpha - \left(f \cos\alpha + D_{pa}\right) Z_i + f D_{pa}}{f - Z_i} \end{cases}. \tag{13}$$

Bringing in formula (5), we can get the following:

$$\begin{cases} X_a = 0 \\ Y_a = \dfrac{-\left(f \sin\alpha + D_{pc}\right)}{X_i \cos\alpha + f \sin\alpha} Y_i \\ Z_a = \dfrac{X_i\left(f + D_{pa}\cos\alpha - D_{pc}\sin\alpha\right) + f\left(D_{pa}\sin\alpha + D_{pc}\cos\alpha\right)}{X_i \cos\alpha + f \sin\alpha} \end{cases}. \tag{14}$$

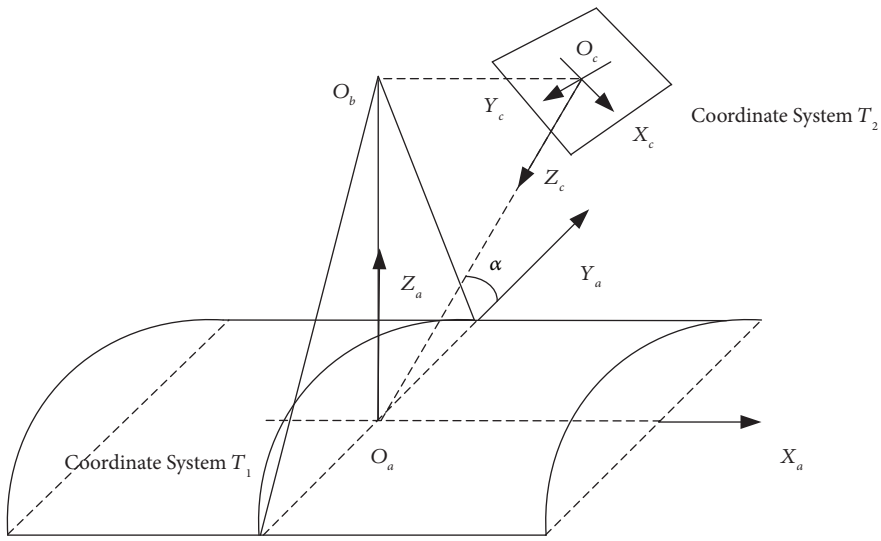

Figure 8: Sensor coordinate system.

Among them is the focal length, D_{pa} and D_{pc} are the sensor structure parameters, which can be obtained through the calibration of the structured light vision sensor, and they can all be regarded as known numbers. By measuring the coordinates of the image plane, it corresponds to the measurement of the object plane.

3. Experiments Using Visual Sensors to Design Public Space Landscape Models

The urban public space landscape plays a vital role in improving the urban ecological environment, beautifying the living environment, improving people's living standards, and improving the urban air quality.

3.1. Image Sensor Interface Initialization. The initialization of the CMOS image sensor [27] is mainly achieved by setting the internal registers of the CMOS sensor through the I2C bus.

Through real-time control of the working status of internal registers, the requirements of image acquisition are realized. In addition, the order should be considered in the setting. The main register settings are shown in Table 1.

The main operations such as initialization of the entire CMOS image sensor and DMA settings are implemented in the initCamera (structcam_cmd_param * ccp) function. We set the ioctl command word CAM_INT, and the application program can initialize the image sensor through this command word, and start image acquisition and other operations. At this point, the image acquisition interface has completed the preparations for receiving data signals.

3.2. Algorithm Simulation Experiment. In a 100 m * 100 m rectangular area, 100 sensor nodes are randomly configured when the communication radius is 15 m. The number of locked nodes in the network is 30, 40, 50, 60, 70, and 80, respectively, and changes in positioning error rate and coverage rate are recorded.

Table 1: The CMOS register function description.

On-chip registers	Symbol mark	Function description
0×001	Row start	Set the CMOS image sensor
0×002	Column start	Acquisition window size
0×003	Output control	Set working mode
0×004	Horizontal blank	Blanking control register
0×005	Vertical blank	
0×006	Read mode 1	Control output data mode
0×007	Read mode 2	

We use the Monte Carlo method to find the location coverage. When the anchor node is 30, the positioning coverage of the APIT algorithm only reaches 10%. This shows that only a very small number of nodes can obtain their own location information, and the effectiveness of the algorithm is very low. This is because the APIT algorithm requires network density and the uniformity of anchor node distribution. The improved algorithm can continuously update the number of anchor nodes in the form of virtual anchor nodes, so even if the number of anchor nodes [28] is small, it can maintain more than 50% position coverage.

3.3. The Design of Modern Public Space from the Perspective of Landscape Architecture Based on Visual Sensors

3.3.1. Site Selection of Public Space. The larger public space in traditional villages is often the center of a village, carrying people's daily production, life, publicity, and gathering. The public space is in the center and important position in terms of location and function.

The newly built public space has the following problems in spatial location selection:

(1) The location is remote; the public space that has just been built now is often built in a new community; and the community is generally remote and far from the villagers' daily life area. This is also one of the

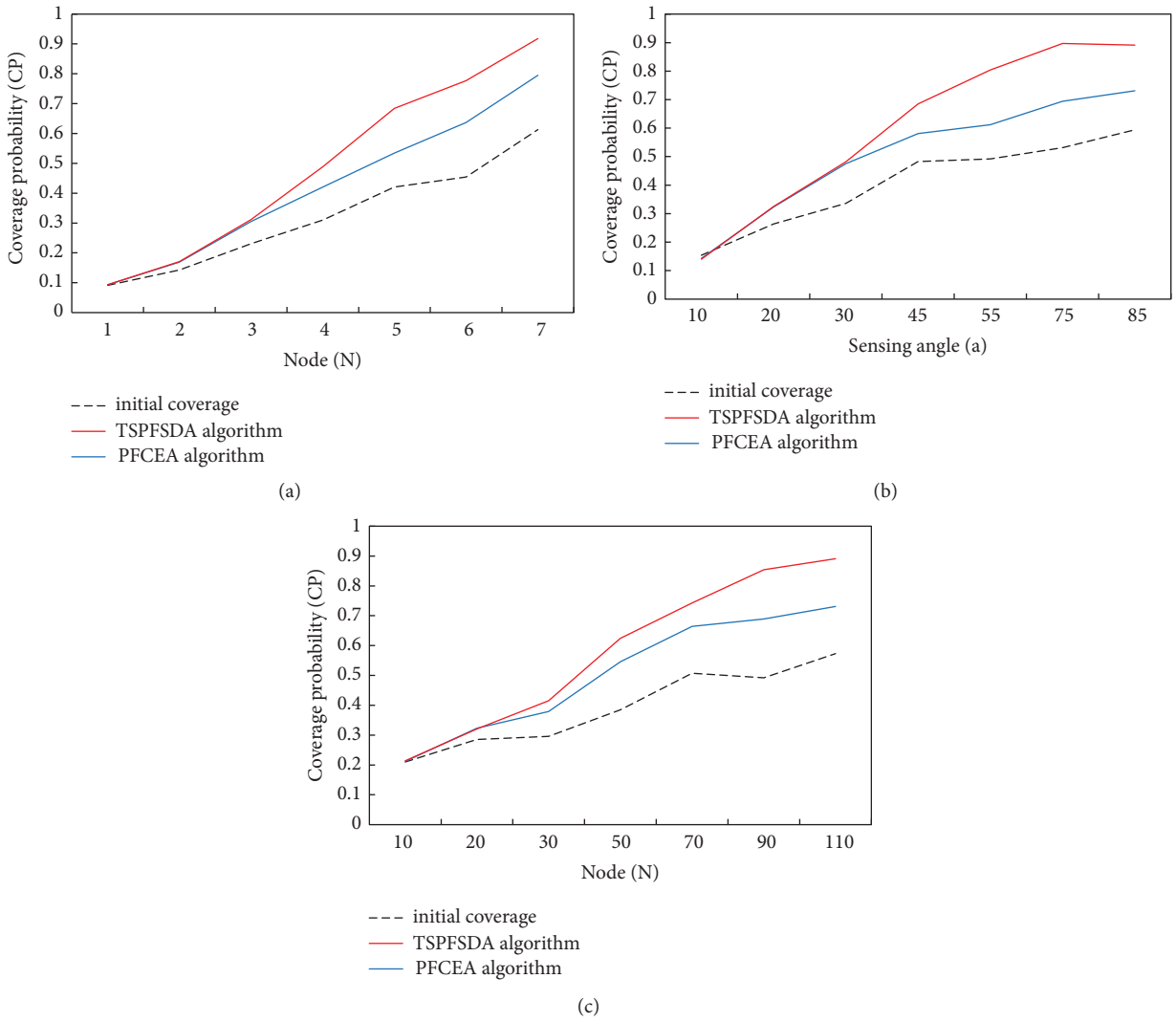

FIGURE 9: The influence of three variables in the simulation experiment. (a) The influence of sensing radius on coverage rate, $N = 70, \alpha = 45^{\circ}, \Delta\theta = 1^{\circ}$. (b) The effect of sensing angle on coverage rate, $N = 70, R = 5, \Delta\theta = 1^{\circ}$. (c) The influence of the number of nodes on the coverage rate $R = 6, \alpha = 45^{\circ}, \Delta\theta = 1^{\circ}$.

reasons why the frequency of public space is not high.

(2) Close to the main road, the traditional villages in Tai'an City have cross-village roads. As the main road of the village, it is the main or even the only passage for foreign exchanges. It has a very strong openness and is an express highway. The public space is selected along the main road. It is by no means the best site selection.

(3) There are few layout points; the traditional villages in Tai'an City are the living mode of detached houses. There are roads between the front and rear houses, and the houses are left and right or next to other households or streets. The house of a family covers an area of about 300 square meters. In summary, a traditional natural village occupies a large area, but most of the villages in the survey have only one newly built public space with relatively complete facilities.

3.3.2. Public Space Scale Design. A space is suitable and not suitable for human use. The sense of scale is the primary criterion. The design of a space scale that is too small will make people who enter the space feel depressed, and a space scale that is too large will make people feel insecure. This study explains the design scale of public space by designing several types. The main types are the internal streets and lanes of the village, the street intersections where residents often gather, and the newly built public activity space mainly composed of fitness facilities.

3.3.3. Plane Layout Design. The plan layout design of public space can be described as diverse depending on the location and the functions undertaken; generally, rectangular space or arc space is the majority. The layout of public space is also divided into two types:

(1) In traditional villages in mountainous areas with more complex topography, the layout of public space

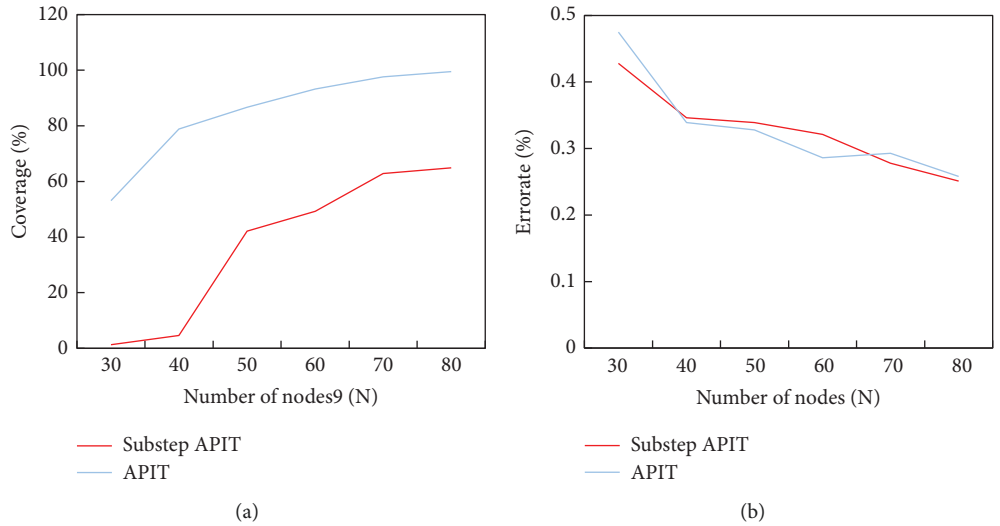

Figure 10: Simulation diagram of the variation curve of the positioning error rate with the anchor node. (a) Positioning coverage rate. (b) Positioning error rate.

Table 2: Sensor measurement value (target true value 900, unit ˚C).

Sensor	Number of measurements					
	1	2	3	4	5	6
1	899.5	905.3	901.9	900.6	889.9	899.4
2	898.3	875.9	888.1	886.2	907.5	904.4
3	896.7	906.8	898.2	904.0	896.4	891.6

Table 3: Comparison of the fusion results of the three methods.

Number of inspections	Mittelungsmethode	Literaturmethode	Methoden in diesem Abschnitt
1	898.1667	898.1667	898.1668
2	896.0000	902.2410	901.7699
3	896.0667	899.9288	900.0086
4	896.9333	900.6016	900.5356
5	897.9333	896.2689	896.7572
6	898.4667	896.1059	896.3125

Table 4: Absolute error comparison of the three methods.

Number of inspections	Mittelungsmethode	Literaturmethode	Methoden in diesem Abschnitt
1	1.8333	1.8333	1.8332
2	4.0000	2.2410	1.7699
3	3.9333	0.0712	0.0086
4	3.0667	0.6016	0.5356
5	2.0667	3.7311	3.2428
6	1.5333	3.8941	3.6875

Table 5: Comparison of the total absolute error of the three methods.

	Total absolute error	Methods
Mittelungsmethode	16.4333	16.5465
Literaturmethode	12.3724	12.4634
Methoden in diesem Abschnitt	11.0776	11.0158

is relatively free and scattered, and the facilities are relatively simple but flexible. The distribution of public space and sites in the village is relatively scattered.

(2) The large traditional villages in the plain area are generally distributed and more concentrated. Generally, comprehensive public places with larger sites are set up at the edge of the village. The comprehensive type refers to the close proximity of different types of public spaces.

3.3.4. Spatial Vegetation Design. From the perspective of human cognition of landscape, landscape generally includes three levels: visual esthetics, spiritual experience, and ecological environment. A good landscape space not only guarantees pleasant landscape facilities but also requires carefully selected plant collocations. The combination of hard and soft landscapes can create a beautiful and suitable landscape environment space. Due to the rich vegetation types and the characteristics of seasonal flowers in different seasons depending on the season, after careful design considerations, planting different types of seasonal flowers or flowering trees and shrubs in different places on the site will make the entire space more landscape design charm and different landscape experience, and experience the design beauty of public space from visual and smell.

4. Experimental Analysis Based on Sensor Design Landscape Model

4.1. Simulation Experiment Analysis. (1) Number of nodes N, sensing radius R, sensing direction(α 4, 5, 6, and 7), and sensing directions (α =10˚, 20˚, 30˚, 45˚, 55˚, 75˚, 85˚) were

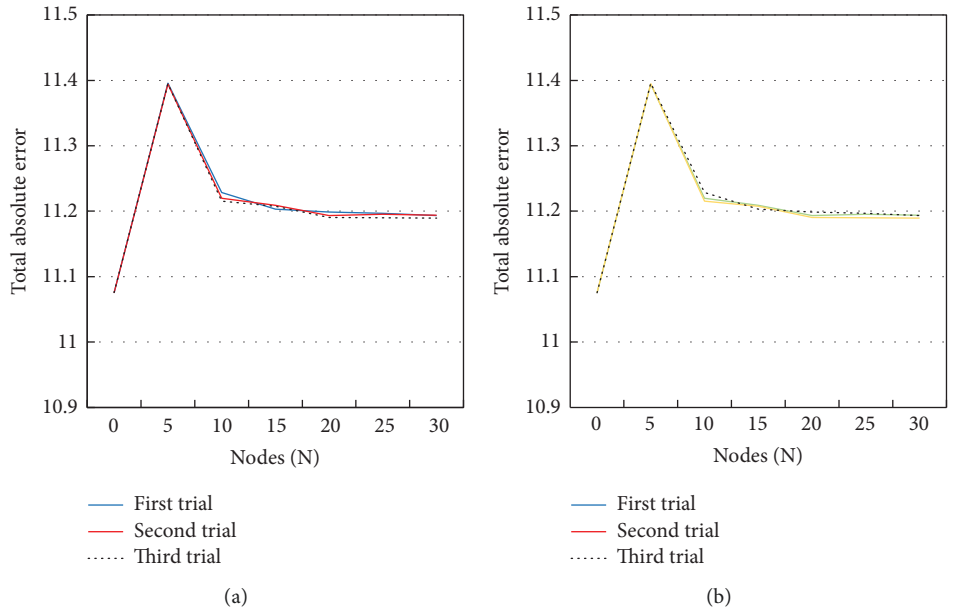

Figure 11: Two error analysis experiments. (a) The first error analysis. (b) The second error analysis.

simulated experiments, and the results are shown in Figure 9.

It can be seen from the experimental simulation results that the performance of the TSPFSDA algorithm proposed in this study is more sensitive to changes in the conditions of the nodes in the sensor network (such as the number of nodes, sensing radius, and sensing angle). Under the premise of the same parameter conditions, the improved algorithm can more effectively increase the coverage area of the network and better distribute the visual nodes evenly in the monitoring area.

The effectiveness of the positioning algorithm cannot only be reflected by the positioning coverage rate [29, 30]. Another important indicator is the positioning error rate. The positioning error rate is calculated using equation (15) [31].

$$\text{error} = \frac{\sum_{i=1}^{n} \sqrt{(a - a_{\text{est}})^2 + (b - b_{\text{est}})^2}}{n * R}. \tag{15}$$

Among them, (a, b) is the true position of the node, $(a_{\text{est}}, b_{\text{est}})$ is the estimated position of the node, n is the number of unknown nodes, and R is the communication radius of the node. The simulation diagrams of the positioning error rate with the anchor node variation curve are shown in Figure 10.

4.2. Comparative Experiment Analysis. Using three thermocouples to measure the temperature of a constant temperature box 6 times, the detected values obtained are shown in Table 2.

Table 3 lists the fusion values calculated using the average method, the literature method, and the algorithm in this section at different detection times [32], and Table 4 lists the average method, the literature method, and the absolute error of the algorithm at different detection times in this section. It can be seen that the absolute error of the algorithm in this section is much smaller than other algorithms. Our extended dimension matrix [33] can comprehensively use the previous detection values to adjust the subsequent fusion weights. Table 5 lists the total absolute error of the six fusion results of the three methods. This table reflects that the total absolute error of the method in this section is smaller than the average method and the literature method.

In order to reflect the stability of this method, we repeated the data in Table 2 many times, increased the number of detections to 200, and then counted the total absolute error of this group for a group of 6 times. The simulation results are shown in Figure 11. From the results of the two experiments, it can be seen that the maximum total absolute error does not exceed 11.4, and the total absolute error tends to stabilize, tending to 11.2.

4.3. The Public Space Landscape Model Is Obtained after 3D Image Processing by the Visual Sensor

(1) Scene Layout

We place 200 vision sensors on the site, connect all sensors, and make relevant preparations.

(2) Collect Pictures

The vision sensor organizes and collects 200 pictures through scanning.

(3) Divide and Organize

Through infrared segmentation technology, the picture is segmented and processed [34], and then, the fusion technology is used to fuse the picture. Through the previous verification and comparison experiments, the error of the integrity of the picture is reduced. Finally, the temperature and time are analyzed to obtain the complete picture. The impact of sex is shown in Figure 12.

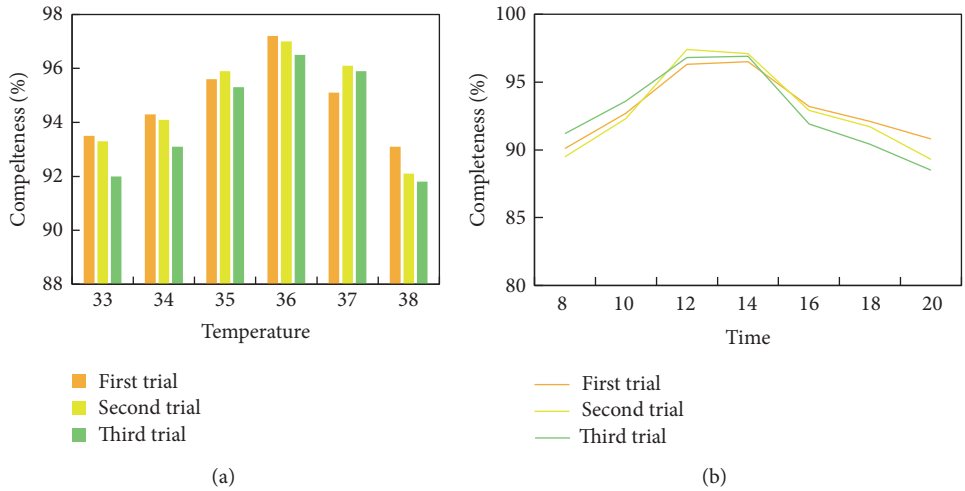

Figure 12: Relationship between completeness and time and temperature. (a) Relationship between integrity and temperature. (b) Relationship between integrity and time.

5. Conclusions

In order to explore the application of visual sensor 3D image in the landscape model of public space, this study starts from the visual sensor and does the operation of many ideas on the sensor. Based on the technology of visual sensor in 3D image processing, the COMS sensor is used to obtain the landscape image from multiple angles, and then, infrared segmentation technology is used to process the image. Then, it is integrated through infrared fusion technology, and finally, the 3D landscape model is sorted and analyzed. This method has strict requirements on temperature and time. The most complete picture can be obtained at the appropriate temperature and time. The temperature is about 35.5°C–36.7°C, the model integrity is as high as 97.2%, and the model integrity is the highest from 12 noon to 2 pm, which can reach 97.1%. Therefore, in order to obtain the most complete public space landscape model, it is best to be from 12 o'clock to 14 o'clock, with a temperature of 35.5°C–36.7°C.

Data Availability

No data were used to support this study.

Conflicts of Interest

The authors declare that there are no conflicts of interest regarding the publication of this article.

References

[1] Z. Yang, S. Lu, T. Wu, G. Yuan, and Y. Tang, "Detection of morphology defects in pipeline based on 3D active stereo omnidirectional vision sensor," *IET Image Processing*, vol. 12, no. 4, pp. 588–595, 2018.

[2] M. Saval-Calvo, J. Azorin-Lopez, A. Fuster-Guillo, V. Villena-Martinez, and R. B. Fisher, "3D non-rigid registration using color: color Coherent Point Drift," *Computer Vision and Image Understanding*, vol. 169, pp. 119–135, 2018.

[3] A. Pujol-Miro, J. R. Casas, and J. Ruiz-Hidalgo, "Correspondence matching in unorganized 3D point clouds using Convolutional Neural Networks," *Image and Vision Computing*, vol. 83–84, pp. 51–60, 2019.

[4] H. Li and C. Zhong, "A machine vision based autonomous navigation system for Lunar rover: the model and key technique," *Sensor Review*, vol. 36, no. 4, pp. 377–385, 2016.

[5] C. Li, B. Lu, Y. Zhang, H. Liu, and Y. Qu, "3D reconstruction of indoor scenes via image registration," *Neural Processing Letters*, vol. 48, no. 3, pp. 1281–1304, 2018.

[6] A. Masson, C. Haskamp, I. Ahrns, R. Brochard, K. Kanani, and R. Delage, "Airbus DS Vision Based Navigation solutions tested on LIRIS experiment data," *Journal of the British Interplanetary Society*, vol. 70, no. 2-3-4, pp. 152–159, 2017.

[7] J. Ma, X. Xiao, R. Bu et al., "Application of the space-for-time substitution method in validating long-term biomass predictions of a forest landscape model," *Environmental Modelling & Software*, vol. 94, pp. 127–139, 2017.

[8] Q. Li, W. B. Chen, J. Zheng, T. Xie, and T. J. Lu, "[Influence of greenspace landscape pattern on $PM_{2.5}$ in the center urban area of Nanchang, China]," *Zhongguo ke xue yuan Shenyang ying yong sheng tai yan jiu suo zhu ban*, vol. 30, no. 11, pp. 3855–3862, 2019.

[9] A. Z. Abualkishik and A. A. Alwan, "Trust aware aquila optimizer based secure data transmission for information management in wireless sensor networks," *Journal of Cybersecurity and Information Management*, vol. 9, no. 1, pp. 40–51, 2022.

[10] C. Barstow, "Imaginative geographies: visualising the poetics of history and space," *Landscapes: The Journal of the International Centre for Landscape and Language*, vol. 8, no. 1, p. 4, 2018.

[11] D. Zheng, K. Liang, fnm au, and K. Liang, "Chaotic butterfly optimization with optimal multi-key image encryption technique for wireless sensor networks," *Journal of Intelligent Systems and Internet of Things*, vol. 1, no. 2, pp. 80–92, 2020.

[12] W. Zhu, H. Wei, L. Chen et al., "Characterization of host plasminogen exploitation of Pasteurella multocida," *Microbial Pathogenesis*, vol. 129, no. 1, pp. 74–77, 2019.

[13] Z. Jian and S. Hao, "Geo-spatial analysis and optimization strategy of park green space landscape pattern of Garden City-A case study of the central district of Mianyang City Sichuan

Province," *European Journal of Remote Sensing*, vol. 53, no. 1, pp. 309–315, 2020.

[14] J. L. Field, E. Marx, M. Easter, P. R. Adler, and K. Paustian, "Ecosystem model parameterization and adaptation for sustainable cellulosic biofuel landscape design," *GCB Bioenergy*, vol. 8, no. 6, pp. 1106–1123, 2016.

[15] I. M. E. El-Hasnony, "Intelligent differential evolution based feature selection with deep neural network for intrusion detection in wireless sensor networks," *Journal of Intelligent Systems and Internet of Things*, vol. 0, no. 2, pp. 78–89, 2019.

[16] A. R. W. Sait, "Trust aware moth flame optimization based secure clustering for wireless sensor networks," *Journal of Intelligent Systems and Internet of Things*, vol. 0, no. 2, pp. 54–64, 2019.

[17] G. M. Street, J. Fieberg, A. R. Rodgers et al., "Habitat functional response mitigates reduced foraging opportunity: implications for animal fitness and space use," *Landscape Ecology*, vol. 31, no. 9, pp. 1939–1953, 2016.

[18] B.-C. Kim, J.-W. Kang, C. Park, and H.-J. Kim, "Analysis of urban heat island (UHI) alleviating effect of urban parks and green space in seoul using deep neural network (DNN) model," *Journal of the Korean Institute of Landscape Architecture*, vol. 48, no. 4, pp. 19–28, 2020.

[19] K. H. Braziunas, R. Seidl, W. Rammer, and M. G. Turner, "Can we manage a future with more fire? Effectiveness of defensible space treatment depends on housing amount and configuration," *Landscape Ecology*, vol. 36, no. 2, pp. 309–330, 2021.

[20] J. Takahashi, K. Masato, S. Ito et al., "Image-retrieval method using gradient dilation images for cloud-based positioning system with 3D wireframe map," *Sensors and Materials*, vol. 32, no. 2, p. 611, 2020.

[21] H. Li and B. Zhang, "Application of integrated binocular stereo vision measurement and wireless sensor system in athlete displacement test," *Alexandria Engineering Journal*, vol. 60, no. 5, pp. 4325–4335, 2021.

[22] J. Li, B. Zhang, X. Kang, W. Xu, G. Yang, and L. Yang, "Single camera 3D digital image correlation using a polarized system," *Instruments and Experimental Techniques*, vol. 61, no. 1, pp. 99–105, 2018.

[23] J. F. P. Kooij, M. C. Liem, J. D. Krijnders, T. C. Andringa, and D. M. Gavrila, "Multi-modal human aggression detection," *Computer Vision and Image Understanding*, vol. 144, pp. 106–120, 2016.

[24] M. Heimberger, J. Horgan, C. Hughes, J. McDonald, and S. Yogamani, "Computer vision in automated parking systems: design, implementation and challenges," *Image and Vision Computing*, vol. 68, pp. 88–101, 2017.

[25] S. Koyama, K. Onozawa, K. Tanaka, S. Saito, S. M. Kourkouss, and Y. Kato, "Multiocular image sensor with on-chip beam-splitter and inner meta-micro-lens for single-main-lens stereo camera," *Optics Express*, vol. 24, no. 16, Article ID 18035, 2016.

[26] Y. Zhong, S. Wang, S. Xie, Z. Cao, K. Jiang, and D. Yang, "3D scene reconstruction with sparse LiDAR data and monocular image in single frame," *SAE International Journal of Passenger Cars - Electronic and Electrical Systems*, vol. 11, no. 1, pp. 48–56, 2017.

[27] C.-J. Liang, K. M. Lundeen, W. Mcgee, C. C. Menassa, S. Lee, and V. R. Kamat, "A vision-based marker-less pose estimation system for articulated construction robots," *Automation in Construction*, vol. 104, pp. 80–94, 2019.

[28] V. Kodukula, S. Katrawala, B. Jones, C.-J. Wu, and R. LiKamWa, "Dynamic temperature management of near-sensor processing for energy-efficient high-fidelity imaging," *Sensors*, vol. 21, no. 3, p. 926, 2021.

[29] K. Makantasis, E. Protopapadakis, A. Doulamis, N. Doulamis, and N. Matsatsinis, "3D measures exploitation for a monocular semi-supervised fall detection system," *Multimedia Tools and Applications*, vol. 75, no. 22, pp. 15017–15049, 2016.

[30] Y. Yin, B. Altmann, C. Pape, and E. Reithmeier, "Machine-vision-guided rotation axis alignment for an optomechanical derotator," *Optics and Lasers in Engineering*, vol. 121, pp. 456–463, 2019.

[31] Y. Hbali, S. Hbali, L. Ballihi, and M. Sadgal, "Skeleton-based human activity recognition for elderly monitoring systems," *IET Computer Vision*, vol. 12, no. 1, pp. 16–26, 2017.

[32] A. M. Pinto, A. P. Moreira, and P. G. Costa, "WirelessSyncroVision: wireless synchronization for industrial stereoscopic systems," *International Journal of Advanced Manufacturing Technology*, vol. 82, no. 5-8, pp. 909–919, 2016.

[33] S. Craciun, R. Kirchgessner, A. D. George, H. Lam, and J. C. Principe, "A real-time, power-efficient architecture for mean-shift image segmentation," *Journal of Real-Time Image Processing*, vol. 14, no. 2, pp. 379–394, 2018.

[34] Y. Wu, Y. Wang, W. Hu, and G. Cao, "SmartPhoto: a resource-aware crowdsourcing approach for image sensing with smartphones," *IEEE Transactions on Mobile Computing*, vol. 15, no. 5, pp. 1249–1263, 2016.